RESEARCH ARTICLE | MAY 02 2025

Dynamics of an active chiral polymer in shear flow

A. Gülce Bayram ; Luca Biancofiore ; Hartmut Löwen

J. Chem. Phys. 162, 174903 (2025)
https://doi.org/10.1063/5.0268723

The Journal of Chemical Physics ARTICLE pubs.aip.org/aip/jcp

Dynamics of an active chiral polymer in shear flow

Cite as: J. Chem. Phys. 162, 174903 (2025); doi: 10.1063/5.0268723
Submitted: 3 March 2025 • Accepted: 4 April 2025 •
Published Online: 2 May 2025

A. Gülce Bayram,[1] Luca Biancofiore,[1,2,a)] and Hartmut Löwen[3]

AFFILIATIONS

[1] Department of Mechanical Engineering, Bilkent University, Çankaya, 06800 Ankara, Turkey
[2] Department of Industrial Engineering Information and Economics, University of L'Aquila, Piazzale Ernesto Pontieri Monteluco di Roio, L'Aquila 67100, Italy
[3] Institut für Theoretische Physik II: Weiche Materie, Heinrich-Heine-Universität Düsseldorf, 40225 Düsseldorf, Germany

[a)] **Author to whom correspondence should be addressed:** luca.biancofiore@univaq.it

ABSTRACT

We explore the complex formation of an active flexible polymer chain in linear shear flow by using monomer-resolved Brownian dynamics simulations in two spatial dimensions. The chiral head monomer is active and circling, while all other monomers are passive, following both the motion of the head polymer and the shear flow. By the combination of activity, chirality, and shear rate, a wealth of different states are found, including the formation of a linear/complex folding and a spiraling state with both head-in and head-out morphologies. As the vorticity of the applied shear competes with the circling sense of the head, the chirality of the whole complex can be tuned by activity. Our results are relevant to characterize the response of living and artificial chiral active polymer chains to complex flow fields.

I. INTRODUCTION

In contrast to their passive counterparts, active polymers[1–3] convert energy taken from the environment into directed motion.[4–7] Among typical examples are living worms,[8–10] filaments,[11–13] artificial chains of granular[14] or colloidal particles,[15–21] and flexible robots.[22] The behavior of active polymers has grown into a modern interdisciplinary research field nested between chemical physics, soft matter science, and biology. In this sense, synthetic active particles have also been designed in several ways to serve as artificial monomers. Phoretic effects due to the local gradients of, e.g., (i) electric, (ii) concentration, and (iii) temperature fields are used to activate these particles.[6,23,24]

Chains of active particles can serve as models for the integrated part of biological systems, e.g., bacterial swarms propelled by flagella. In these studies, activity is observed to play a crucial role in the formation of stable rotating spiral coils, as well as in controlling their folding and unfolding processes.[25] Other interesting new phenomena are activity-induced chain swelling[26,27] and collapsing,[18,26] as well as the spontaneous formation of spirals[28] and a change of the scaling exponents relative to passive polymers.[29] Moreover, although the influence of activity on stiff polymers is severe, it induces a transition from semiflexible-polymer behavior to flexible-polymer behavior with increasing activity.[30]

When passive polymers are exposed to shear flow, they start to tumble, and the sense of the rotation of the whole chain is governed by the vorticity direction of the imposed shear field. The underlying physics is by now well understood.[31–36] The behavior of sheared active polymer chains is more intricate and has been addressed only recently by theory and simulation.[37–40] Novel properties of the polymer conformations induced by a combination of activity and shear have been reported, including significant deviations from passive scaling laws. The combination of fluid-flow and active forces gives rise to fascinating phenomena in the swimming route of micro-organisms, such as upstream swimming[41,42] and vorticity migration.[43] In addition, activity induces significant alterations in viscosity under shear flow, as observed in bacterial systems[44] and colloidal suspensions.[45] This characteristic makes active polymers, or polymer-like structures, intriguing candidates as rheology modifiers in natural or industrial[46,47] applications.

Here, we introduce the concept of chirality to a sheared active polymer. Instead of being self-propelled linearly, leading to straight motion, active particles can also spin and circle.[48–50] There are two ways to connect chirality to active matter:[51] either a single particle is already chiral, such that chirality is observed for the trajectories of individual particles,[52,53] or collections of non-chiral particles spontaneously self-organize into chiral structures.[28,54–57] In the first case, chirality is imposed; in the latter, it is spontaneously emerging.

In this paper, we consider a single active polymer in shear flow that has an imposed chiral head monomer such that this monomer is moving in a circle.[58,59] The rest of the polymer chain is passive, following the moving head but exposed to the shear flow. Therefore, there is a combination and competition of activity, chirality, and shear flow. Using monomer-resolved Brownian dynamics computer simulations in two dimensions, we explore the complex formation of such a flexible polymer chain and its rheological properties. We find a plethora of different conformations, including linear stretched complexes and spiraling states. The head monomer is either engulfed by the rest of the chain or rotating around the other monomers. As the vorticity of the applied shear competes with the circling sense of the head, the chirality of the whole complex can be tuned both by activity and the shear rate. Our results can be verified on artificial model granular or colloidal chiral chains exposed to shear and are of importance in characterizing the response of living chiral active polymers to complex flow fields. This paper is organized as follows: Sec. II provides a description of our model. Results are presented in Sec. III and conclusions are drawn in Sec. IV.

II. METHODS

We study an active polymer chain with a chiral head under linear shear flow, as schematically illustrated in Fig. 1, with blue arrows indicating the flow gradient in the y-direction. In Sec. II A, we explain the model employed to simulate this system, followed by a description of the simulation parameters utilized in the system simulation in Sec. II B.

A. Model

We use Brownian dynamics to model a linear polymer chain, described as a sequence of N_m coarse-grained spring beads in two spatial dimensions. We label each monomer by an integer index i, where the active head monomer has $i = 1$ and all other passive monomers are indexed with $i = 2, 3, \ldots, N_m$. In the presence of a steady shear rate $\dot{\gamma}$, the translational motion of the passive monomers ($i \neq 1$) in the overdamped limit (corresponding to Brownian dynamics at zero temperature) is given by

$$\dot{\mathbf{r}}_i = -\frac{1}{\Gamma}\sum_{\substack{j=1\\ j\neq i}}^{N_m} \nabla_i U_{ij} + \dot{\gamma} r_{i,y}\mathbf{e}_x, \tag{1}$$

and the motion of the active head monomer is described by

$$\dot{\mathbf{r}}_1 = -\frac{1}{\Gamma}\sum_{j=2}^{N_m} \nabla_1 U_{1j} + \dot{\gamma} r_{1,y}\mathbf{e}_x + v_0\mathbf{e}_h, \tag{2}$$

where $\mathbf{r}_i = (r_{i,x}, r_{i,y})$ denotes the position vector of the i-th monomer, and Γ is the translational friction coefficient. The second term on the right-hand side of the equations is the uniform linear *shear flow* imposed in the x-direction with unit vector $\mathbf{e}_x$ such that the shear gradient is along the y-axis.

Since the chiral head monomer ($i = 1$) is active, it moves additionally with the constant active speed v_0 in the direction described by the unit vector $\boldsymbol{e_h} = (\cos\theta_h,\ \sin\theta_h)$,[18,30] which we refer to as *activity*. Here, θ_h denotes its orientational angle with the x-axis. Then, its translational equation of motion can be written as Eq. (2). The orientation of the head monomer is governed by the rotational equation of motion,[60]

$$\dot{\theta}_h(t) = -\frac{\dot{\gamma}}{2} - \omega_c. \tag{3}$$

Here, $\dot{\gamma}/2$ denotes the shear-induced rotation of a sphere (i.e., with the term $\dot{\gamma}/2$ we take into account the rotational motion of an isolated particle subjected to a shear flow[61]), and ω_c is a rotation frequency internally or externally forced by a torque on the head monomer. We refer to this frequency as the head *chirality*. This frequency controls how fast the orientation of the head monomer changes and, consequently, it can set the whole complex into overall rotation. It can be realized experimentally in various ways. For instance, the head monomer can carry a dipole moment and be brought into rotation either by a rotating magnetic field[62–64] or by circularly polarized light.[65]

The first term on the right-hand side of Eqs. (1) and (2) accounts for all the conservative forces acting on the i-th monomer, including the excluded-volume and bond interactions. The excluded-volume interactions between the monomers are described by a smooth repulsive Weeks–Chandler–Andersen (WCA) potential,[66]

$$U_{WCA}(r) = \begin{cases} 4\varepsilon\left[\left(\frac{\sigma}{r}\right)^{12} - \left(\frac{\sigma}{r}\right)^{6}\right] + \varepsilon, & r \le 2^{1/6}\sigma, \\ 0, & r > 2^{1/6}\sigma. \end{cases} \tag{4}$$

Here, σ is the diameter of the monomers, and ε is the interaction strength. The spring connection of neighboring monomers is introduced via a FENE (finitely extensible nonlinear elastic) potential,[18,67]

$$U_{FENE}(r) = -\frac{1}{2}KR_0^2 \ln\left[1 - \left(\frac{r_{ij}}{R_0}\right)^2\right], \tag{5}$$

where i and j are the neighboring beads with their distance being $r_{ij} = |\mathbf{r}_i - \mathbf{r}_j|$. The spring constant is $K = 27\varepsilon/\sigma^2$, while the maximum allowed bond length is $R_0 = 1.5\sigma$.

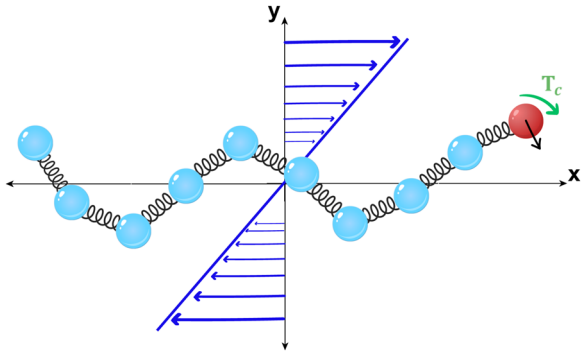

FIG. 1. Schematic of an active bead–spring polymer with a chiral head (red monomer) in the linear flow. The blue monomers are passive. The black arrow on the head monomer represents the direction of the active force, and the green arrow depicts the direction of head chirality. The flow is imposed along the x-axis, and the gradient is in the y-direction, whose variation is shown by blue arrows.

B. Simulation parameters

In our simulations, we use σ and ε as our units of length and energy, respectively, while we measure time in units of the characteristic time $\tau_0 = \Gamma\sigma^2/\varepsilon$. The number of monomers in the polymer is set to $N_m = 20$. The overdamped equations of motion, Eqs. (1)–(3), have been integrated with a small finite time step $\Delta t = 10^{-4}\tau_0$, assuming periodic boundary conditions. The dimensions of the computational box are chosen as $L_x, L_y = (80\sigma, 40\sigma)$.

The dimensionless activity is $v_0\tau_0/\sigma$, which varies in the range of [0.1, 100], while the dimensionless shear rate $\dot{\gamma}\tau_0$ is chosen in the range of [0.01, 50]. In addition, positive values of both the dimensionless shear rate and the external torque in Eq. (3) rotate the head monomer clockwise, as shown in Fig. 1, but we also use negative values of the dimensionless shear rate for the analyses in Sec. III C. Even in the absence of noise, the system runs into a dynamic state that does not depend on the initial conditions. It is this state that we shall analyze in the sequel.

III. RESULTS

Equipped with a chiral head, the active flexible polymer chain exhibits various conformational states under shear flow. The shear triggers the translational motion of the chain by similarly affecting all the monomers. Thus, the polymer chain tends to move aligned with the flow. Since the chiral head monomer is active, it circles due to both shear torque and its head chirality. This section elucidates the conformational states and the interplay between shear vorticity and head chirality by also addressing the rheological properties. In Secs. III A–III D, we analyze the system in the case of vanishing translational and rotational diffusion coefficients, while in Sec. III E, we include thermal or environmental fluctuations.

A. Combined effect of head activity and shear rate on the polymer conformation

We examine a flexible polymer chain that has an active head with a constant clockwise chirality of $\omega_c\tau_0 = 2$. While the chiral head circles, all other passive monomers both (i) follow the head monomer via the connecting polymer bonds and (ii) flow with the shear. We identify two main regimes: *folding* and *spiraling* for the shear-dominated and activity-dominated cases, respectively, which are observable only when the head monomer is active. Here, the activity leverages the chiral motion of the head, thereby controlling the polymer regimes under shear flow (see Fig. 2). Applicable to all states, we observe a range of conformational diversity as activity increases at the same shear rate.

Up to the intermediate values of $v_0/\dot{\gamma}\sigma$, we observe the shear-dominated regime, in which the chain folds into two distinct forms: *linear folding* and *complex folding*. In the linear folding regime, a weak activity can only initiate a subtle clockwise rotation, and the head monomer is subsequently entrained by the negative flow field beneath the centerline, inducing movement of the chain along the flow. This results in the folding of the chain (depicted by ▸ in Fig. 2); where the further rotation of the head monomer halts by the passive tail (see S1.mp4 in the supplementary material).

As the activity increases, the swirling motion of the head monomer becomes intense, exerting greater influence over the entire chain. When the head folds the chain once, the rotation of the head is not blocked by the passive monomers it encounters along its path. Instead, the head monomer pushes and rearranges the passive monomers around itself, leading to the formation of a complex folding pattern (indicated by all ▾ in Fig. 2); see S2.mp4 in the supplementary material videos. Thus, the head monomer is surrounded by the passive monomers, forming a cavity. However, the shear flow compresses the chain conformation in the shear gradient direction and stretches the cavity from its corners to align it along the flow direction. This shear-induced conformation of an active chain due to stretching/alignment in the flow direction and compression in the gradient direction is similar to what was observed previously in the case of all monomers being active.[68]

When activity dominates, the spiraling state of the chain is enabled. At the beginning of activity dominance, the head continues its enclosed rotations within the cavity, akin to complex folding. Differently, the chain activity overcomes the compression and alignment effects of the shear flow on the chain conformation and achieves a perfect circular form, referred to as head-in spiraling (indicated by ▲ in Fig. 2); see S3.mp4 in the supplementary material. In this range, increasing the head activity widens the diameter of the circling, creating a larger inner cavity.

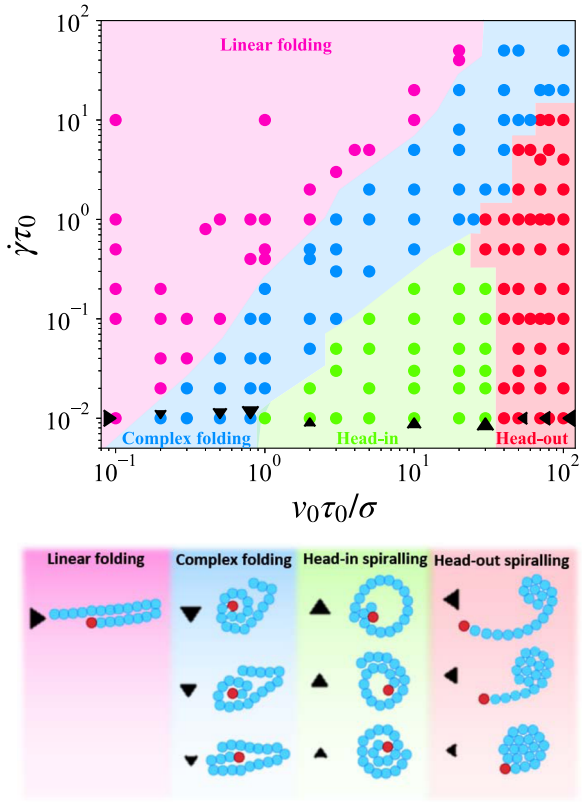

FIG. 2. State diagram of the active polymer chain conformations as a function of activity $v_0\tau_0/\sigma$ and shear rate $\dot{\gamma}\tau_0$ for $\omega_c\tau_0 = 2$: linear folding (magenta), complex folding (blue), head-in spiraling (green), and head-out spiraling (red). The conformational diversity of the states is demonstrated underneath the diagram. Their corresponding parameters are marked by black symbols in the state diagram.

On the other hand, the size of the inner cavity is constrained by the length of the polymer chain. When the head monomer rotates with a diameter larger than the maximum diameter achievable by the chain's length, it escapes from the cavity and, in turn, encapsulates the passive monomers (see all ◂ in Fig. 2). We denote this motion of the chain as head-out spiraling; see also S4.mp4 in the supplementary material. Generally, in both spiraling regimes (head-in and head-out), the activity drives the encapsulation process, while the shear flow instigates the rolling of the polymer chain as a bulk along the flow direction. Appendix A also compares the effect of the chain length on the appearance of these regimes on the state diagram.

B. Dynamics of the gyration diameter

Conformational properties of the active polymer can be conveniently characterized by the radius of gyration,

$$R_g^2 = \frac{1}{N_m}\sum_{i=1}^{N_m}(\mathbf{r}_i - \mathbf{r}_{cm})^2, \tag{6}$$

where $(\mathbf{r}_i - \mathbf{r}_{cm})$ is the position of the ith monomer in the polymer center-of-mass reference frame, with $\mathbf{r}_{cm} = \sum_{i=1}^{N_m}\mathbf{r}_i$. The mean square radius of gyration is then $\overline{R}_g^2$. The overline denotes a time average.

Figure 3(a) shows the change in radius of gyration of four different conformational states over time, where the active polymer chain undergoes either folding or spiraling in a cyclic fashion. In the linear folding conformation, the mean radius of gyration fluctuates around the size of the polymer chain. R_g^2 exceeds the chain size due to the stretching of the chain during its linear extension, while R_g^2 decreases below that during the subsequent linear folding. The duration of these plateaus in R_g^2 indicates the extent of chain stretching: longer plateaus correspond to greater stretching by shear.

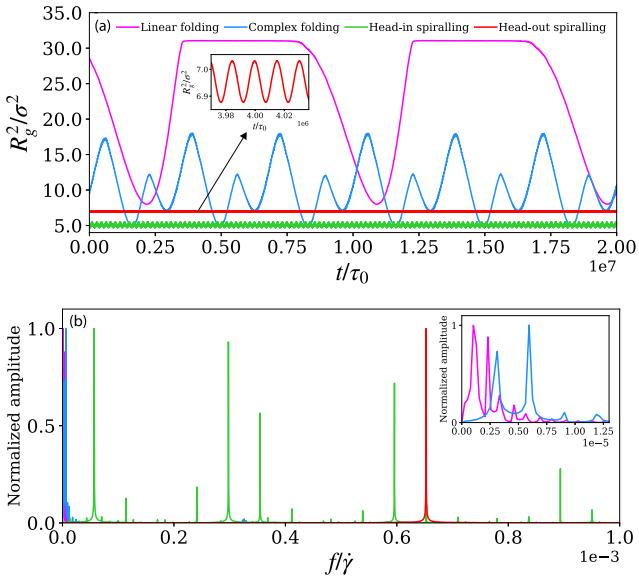

FIG. 3. (a) Square of the radius of gyration R_g^2 as a function of reduced time t/τ_0 in the steady state: linear folding ($v_0\tau_0/\sigma = 0.1, \dot{\gamma}\tau_0 = 0.1$), complex folding ($v_0\tau_0/\sigma = 1, \dot{\gamma}\tau_0 = 0.1$), head-in spiraling ($v_0\tau_0/\sigma = 20, \dot{\gamma}\tau_0 = 0.1$), and head-out spiraling ($v_0\tau_0/\sigma = 80, \dot{\gamma}\tau_0 = 0.1$). (b) Fourier spectra of $R_g^2(t)$ (in arbitrary units) as a function of reduced frequency $f/\dot{\gamma}$ indicating the characteristic frequency peaks related to the polymer state. The colors are used to match the states, as in Fig. 2.

Comparing the linear and complex folding regimes, we observe that the encapsulation of the head monomer produces a secondary peak characterizing the head rotation within the cavity. For spiraling regimes, the radius of gyration shows periodic oscillations while being comparably smaller.

We plot the corresponding Fourier spectra of $R_g^2(t)$ in Fig. 3(b). In the folding states, the two primary peaks have different relative weights (see the inset). For the spiraling states, the frequency of the head swirling gets considerably higher due to dominant activity, resulting in shifted swirling peaks in the spectrum to higher frequencies. Particular to the head-out spiraling state, we observe a single peak in the Fourier spectrum.

Figure 4(a) displays the mean radius of gyration $\overline{R}_g^2$ with increasing activity for several shear rates. A polymer chain in folding states exhibits a descending trend of $\overline{R}_g^2$ as the activity increases. This suggests that higher activity leads to more effective chain folding. Larger $\overline{R}_g^2$ under higher shear flows is observed for the chains with the same activity due to the further stretching effect of shear. At the transition to the head-in spiraling state, $\overline{R}_g^2$ evolves into an ascending trend. This transition occurs at lower activities at low shear, as it becomes easier for the activity to dominate. Within the activity range of the head-in spiraling, the mean radius of gyration keeps increasing due to the expansion of the cavity, as observed in the state diagram (Fig. 2). In the head-out spiraling state, $v_0\tau_0/\sigma > 30$, the mean radius of gyration becomes independent of the shear rate, and the chain conformation depends only on activity. Initially, $\overline{R}_g^2$ seems to decrease smoothly due to the unstable conformations at the beginning of the state (the smallest ◂ in Fig. 2), in which the head monomer intermittently attempts to leave the encapsulated monomers. This results in a larger mean radius of gyration than the fully wrapped conformation occurring at slightly larger activities. The stabilization of the head-out state occurs at activities $v_0\tau_0/\sigma \sim 60$, where the minimum $\overline{R}_g^2$ is reached. Subsequently, as the size of the encapsulated passive monomers decreases with activity (as illustrated by ◂ symbols in Fig. 2), $\overline{R}_g^2$ starts increasing.

Figure 4(b) shows the frequency of the highest amplitude peak at the Fourier spectra, i.e., the highest frequency peak f_c, normalized by the corresponding shear rates $\dot{\gamma}$, plotted as a function of activity. The folding frequency is lower than that of spiraling states and increases slightly as activity increases. Later, the transition to the head-in spiraling state is identified by a frequency jump. Thereafter, the characteristic frequency of the head-in spiraling state remains constant with activity. However, this plateau occurs at higher frequencies for lower shear rates. This again highlights the dominance of the activity, which further increases the head swirling frequency within the cavity when the shear is weaker. For $\dot{\gamma} = 1$, the head-in spiraling state is absent (see Fig. 2); we lose the first jump in the normalized frequencies. Similarly, the transition to the head-out state is identified by the second jump to a constant characteristic frequency, which remains unaffected by activity. The data shown in Figs. 4(a) and 4(b) provide evidence to characterize regime transitions. In addition, they demonstrate how the size of the conformation and the folding/spiraling frequencies are tuned by (i) the activity of the chain and (ii) the imposed shear flow. Similar to the active polymer

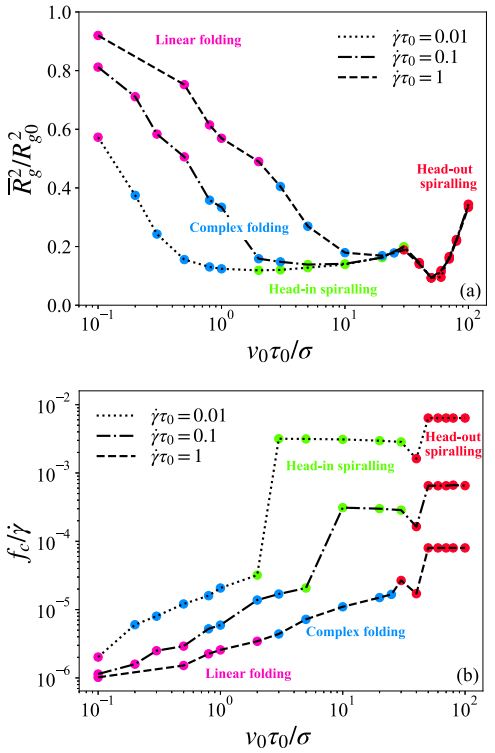

FIG. 4. (a) Normalized mean-square radius of gyration $\overline{R}_g^2/R_{g0}^2$, where R_{g0}^2 is the mean-square radius of gyration of the polymer at $v_0\tau_0/\sigma = 0$ and $\dot{\gamma}\tau_0 = 0$, and (b) the normalized characteristic frequency f_c obtained from the Fourier spectra of R_g^2-time data as a function of activity $v_0\tau_0/\sigma$ for $\dot{\gamma}\tau_0 = 0.01$, 0.1, and 1. The symbols denote the state of the active polymer chain at the corresponding states: linear folding (magenta), complex folding (blue), head-in spiraling (green), and head-out spiraling (red).

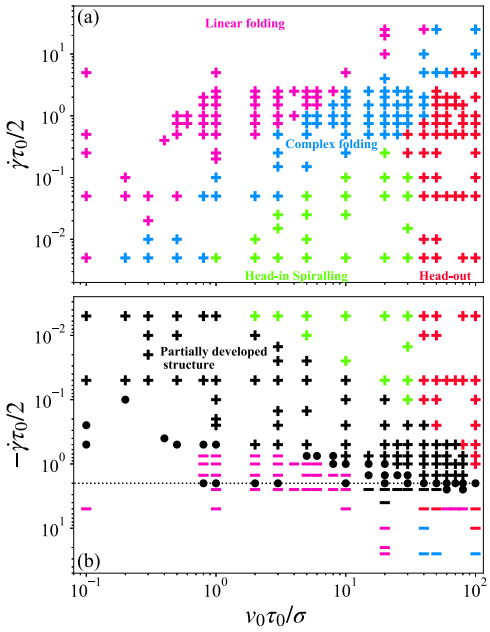

FIG. 5. (a) State diagram when both frequencies cause clockwise rotation of the head monomer, $\dot{\gamma}\tau_0/2 > 0$ and $\omega_c\tau_0 > 0$. (b) The state diagram when the shear flow creates a counterclockwise shear torque on the monomer, $\dot{\gamma}\tau_0/2 < 0$, while the head chirality resists the clockwise rotation with $\omega_c\tau_0 > 0$. The colorcode represents different states: linear folding (magenta), complex folding (blue), head-in spiraling (green), head-out spiraling (red), and partially developed states (black). Symbols correspond to clockwise (+), counterclockwise (−), and hesitant (•) rotations. The dotted black line denotes the neutralization of the countercurrent torques on the head monomer for high activities.

chain composed solely of active monomers,[13,68] we note a consistent trend in $\overline{R}_g^2$ with increasing activity $v_0\tau_0/\sigma < 30$. However, beyond this activity threshold, we observe that the combination of activity and chirality of the head monomer reveals a distinct spiraling state unique to active polymer chains with a chiral head.

C. Competition between shear rate and head chirality

In this section, we shift our focus to the competition between two frequencies, the shear-induced eigen-rotation $\dot{\gamma}/2$ and the frequency ω_c stemming from the head chirality, in determining the final direction of both folding and spiraling conformations. In this way, the response of the active polymer is better understood under different operating conditions (for instance, different shear flow directions or head monomer spin directions), which helps in the experimental realization of this system in the future. To do that, these frequencies (respectively, torques), which are tunable by external forces in the system, are applied countercurrently. Figure 5 shows the conformational state diagrams where both torques are clockwise in (a) and the opposite case (i.e., counterclockwise shear torque vs clockwise chiral torque in (b).

In Fig. 5(a), the active polymer chain forms the conformational states consistently in a clockwise direction, as previously observed (see Fig. 2). While, in Fig. 5(b), we obtain a different state diagram when the same active polymer with a clockwise head chirality is simulated under the shear reversed flow field [$\dot{\gamma} < 0$ used in Eqs.(1)–(3)], resulting in counterclockwise shear torque. When activity dominates, the head chirality prevails over the shear torque, allowing the head-in and head-out spiraling states to persist mostly on the state diagram. However, as the shear flow increases or the polymer activity decreases, the shear torque resists the head chirality more, destroying the complex folding state. Despite the head monomer's overall tendency to rotate the polymer chain clockwise, this competition allows only partially developed polymer chain structures (see S6.mp4 in the supplementary material). At a point, the head monomer also loses a clockwise rotational tendency and reveals a "hesitant" state. Around this hesitancy on the state diagram, the head monomer keeps attempting to rotate the chain in a clockwise direction (+) in the activity dominant regions of the state diagram, while in a counterclockwise (−) direction in the shear dominant regions. However, the hesitant state arises due to the balanced effects of shear and activity, wherein the polymer remains linear.

When the magnitudes of two countercurrent torques become exactly equivalent, such that $\dot{\gamma}\tau_0/2 = -2$ and $\omega_c\tau_0 = 2$ in Eq. (3), the active polymer chain remains always linear without any directional preference of the head monomer over the range of activities

[see the dotted line in Fig. 5(b)]. Consequently, it only translates with the shear flow. Below this torque neutralization line on the state diagram, since shear prevails in the system, the shear torque $\dot{\gamma}/2$ surpasses the head chirality T_c. As a result, either the shear-dominant or hesitant states emerge in a counterclockwise direction. The effect of different head chirality on the state diagram is further analyzed with different ω_c values in Appendix B.

D. Viscosity of the polymer

The rheological response of the active polymer chain with a chiral head is characterized by the shear viscosity, η, which is calculated via shear stress according to

$$\sigma_{xy} = -\frac{1}{\Omega}\sum_{i=1}^{N_m}\sum_{i>j}\frac{\partial U}{\partial r_{ij}}\frac{r_{ij,x}}{r_{ij,y}}r_{ij}, \tag{7}$$

where $r_{ij,x}$ and $r_{ij,y}$ are the distances between the centers of two particles i and j in the direction of x and y, respectively, while $\Omega = L_x L_y$ is the system area. The shear stress is nondimensionalized by considering the energy and length scales, ε and σ, of the system. The shear viscosity is then calculated as $\eta = \overline{\sigma}_{xy}/\dot{\gamma}$.

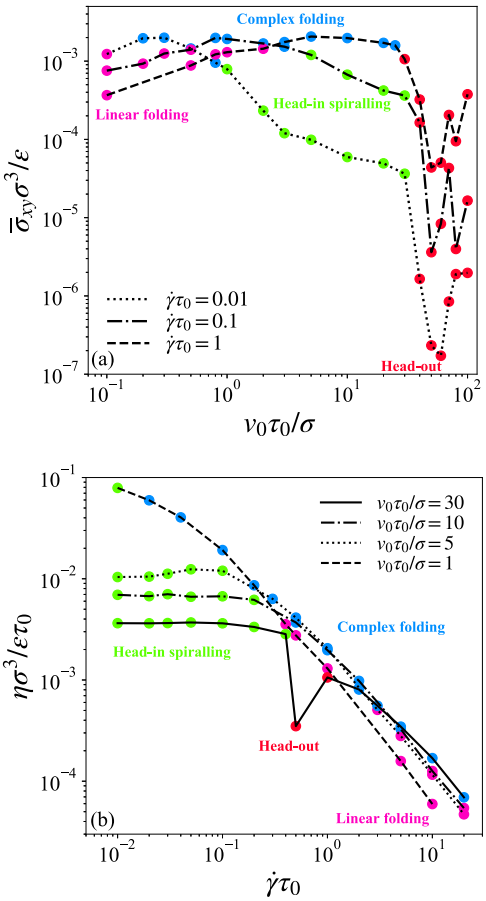

FIG. 6. (a) Nondimensional shear stress $\sigma_{xy}\sigma^3/\varepsilon$ as a function of the chain activity $v_0\tau_0/\sigma$ for various shear rates, $\dot{\gamma}\tau_0 = (0.01, 0.1, 1)$. (b) Nondimensional shear viscosity $\eta\sigma^3/\varepsilon\tau_0$ as a function of shear rate $\dot{\gamma}\tau_0$ for the polymer chain activities $v_0\tau_0/\sigma = (30, 10, 5, 1)$. The symbols denote the state of the active polymer chain at the corresponding states: linear folding (magenta), complex folding (blue), head-in spiraling (green), and head-out spiraling (red).

Figure 6(a) displays the shear stress as a function of activity for various shear flows, highlighting the contribution of different polymer conformations to the shear stress. The two folding states of the polymer chain demonstrate distinct contributions to the shear stress. Chain folding increases the shear stress compared to the linear polymer chain simply flowing under the shear flow.[69] Here, the chain in the linear folding state ($\star$ symbols) increases the shear stress until crossing to a complex folding form ($\bullet$ symbols). Immediately after this crossover, the chain reaches the maximum stress, allowing us to discriminate the folding states.

Moreover, the shear stress contribution of the polymer chain in the complex folding state tends to remain more constant with the activity, especially in the case of the absent head-in spiraling regime due to the balance between activity and shear ($\dot{\gamma}\tau_0 = 1$). When the activity-induced forces on the chain surpass the shear forces, the chain directly translates into the head-out spiraling, resulting in a sharp decrease in shear stress. Conversely, when the head-in spiraling state is present, such as $\dot{\gamma}\tau_0 = 0.01$ and $\dot{\gamma}\tau_0 = 0.1$ on Fig. 6(a), the shear stress initially decreases smoothly with increasing activity before the transition from folding to spiraling occurs. In both cases, during this transition, the activity assists the polymer chain in relaxing the stress, enabling it to flow with shear as a bulk unit. An additional influence of the conformational diversity in the head-out spiraling state is observed, resulting in an oscillating response on the state diagram at large activities.

Moreover, we also observe that the activity severely affects the intrinsic viscosity of the polymer in Fig. 6(b). At low activity, $v_0\tau_0/\sigma = 1$, the polymer chain consistently behaves as a shear thinning fluid, wherein the viscosity decreases with increasing shear rate. Its decrease in η reflects the alignment and the stretching of the polymer chain in the folding states due to the shear dominance, hence resulting in a more pronounced viscosity change. Through the moderate activities, $v_0\tau_0/\sigma = 5 - 10$, the polymer behaves as a Newtonian fluid at low shear rates $\dot{\gamma}\tau_0 < 0.1$, showing shear rate-independent viscosity. In this range, the chain predominantly adopts the head-in spiraling state. However, as the shear rate rises, the chain behavior turns into shear thinning as the chain enters the folding state. These results with an active chiral polymer chain show agreement with the previous simulations conducted on a chain composed only of active monomers.[68] On the other hand, for a more active polymer chain, i.e., $v_0\tau_0/\sigma = 30$, a smooth transition from Newtonian to shear thinning behavior is disrupted by an unstable head-out spiraling conformation of the chain observed around $\dot{\gamma}\tau_0 = 0.4$ (see S5.mp4 in the supplementary material). Although we expect the head-out spiraling state to reveal weaker flow resistance, the unstable conformation makes it significantly weaker. In general, we observe that the rheological transition from Newtonian to shear thinning behavior of the chain occurs at higher shear rates when the chain activity increases. The folding polymer chain exhibits shear thinning behavior, whereas the head-in spiraling polymer chain behaves as a Newtonian fluid. The further activity induces a kind of shrinkage effect on the spiraling polymer chain conformation by weakening the importance of excluded-volume interaction among the monomers and the shear flow, leading to a more shear-independent viscosity response.

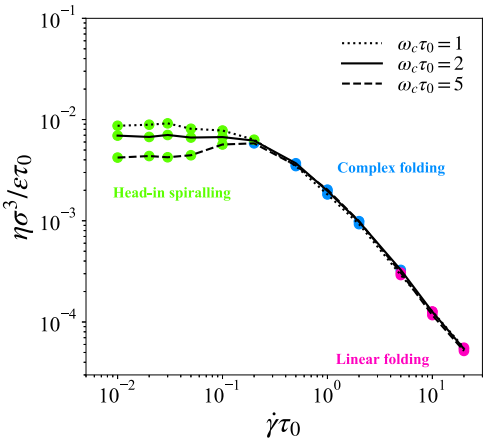

FIG. 7. Nondimensional shear viscosity $\eta\sigma^3/\varepsilon\tau_0$ as a function of shear rate $\dot{\gamma}\tau_0$ for a head monomer with fixed activity $v_0\tau_0/\sigma = 10$ at different chiralities $\omega_c\tau_0 = 1, 2, 5$. The symbols denote the state of the active polymer chain at the corresponding states: linear folding (magenta), complex folding (blue), head-in spiraling (green), and head-out spiraling (red).

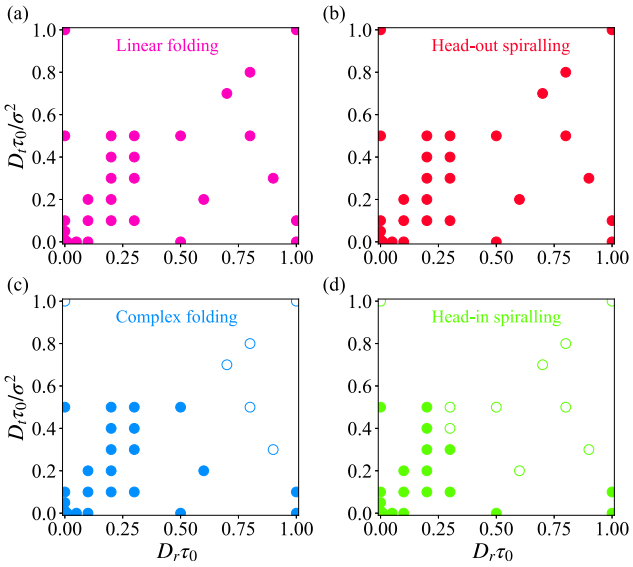

FIG. 8. Appearance of the conformational states of the active polymer chain in the presence of translational and rotational fluctuations: (a) linear folding ($v_0\tau_0/\sigma = 1$, $\dot{\gamma}\tau_0 = 10$), (b) head-out spiraling ($v_0\tau_0/\sigma = 80$, $\dot{\gamma}\tau_0 = 0.1$), (c) complex folding ($v_0\tau_0/\sigma = 10$, $\dot{\gamma}\tau_0 = 1$), and (d) head-in spiraling ($v_0\tau_0/\sigma = 10$, $\dot{\gamma}\tau_0 = 0.1$) states. The colorcode represents the different states, matching the state diagrams. The closed (●) and open (○) symbols denote the appearance and disappearance of the corresponding states, respectively.

To further understand the role of chirality in rheology, we analyze the dependence of viscosity on the chirality ω_c at a fixed activity level $v_0\tau_0/\sigma = 10$. Figure 7 presents the variation of viscosity with ω_c as a function of the shear rate. At high shear rates, where the folding states are favored, viscosity follows a shear-thinning trend independent of chirality, suggesting that strong shear dominates over chiral effects. At moderate shear rates, chirality becomes more influential as it competes with self-propulsion in the stress dissipation. At low shear rates, where the system transitions to a spiraling state with a clear Newtonian behavior, viscosity decreases with increasing ω_c, indicating that a further rotational motion weakens the shear alignment, thereby reducing resistance to flow. These findings provide a more comprehensive understanding of how chirality influences the stress dissipation in active polymer systems. By complementing our previous analysis, they highlight the intricate interplay between these three factors in shaping the system's non-equilibrium rheology.

E. Effect of fluctuations

We next investigate the existence of the same polymer conformational states when including thermal or environmental fluctuations (shown in Fig. 8). Therefore, we include the Gaussian random processes (ξ_i) and (η_h) via non-zero translational (D_t) and rotational (D_r) diffusion coefficients in the overdamped equations of motion as follows:

$$\dot{\mathbf{r}}_i = -\frac{1}{\Gamma}\sum_{\substack{j=1\\ j\neq i}}^{N_m} \nabla_i U_{ij} + \dot{\gamma} r_{i,y}\mathbf{e}_x + \xi_i, \tag{8}$$

$$\dot{\mathbf{r}}_1 = -\frac{1}{\Gamma}\sum_{j=2}^{N_m} \nabla_1 U_{1j} + \dot{\gamma} r_{1,y}\mathbf{e}_x + \xi_1 + v_0\mathbf{e}_h, \tag{9}$$

$$\dot{\theta}_h(t) = \eta_h - \frac{\dot{\gamma}}{2} - \omega_c. \tag{10}$$

$\xi_i(t) = (\xi_{i,x}, \xi_{i,y})$ is a Gaussian white noise term, describing the thermal fluctuations affecting all monomers in the system with zero mean and the correlation $\langle \xi(t)\xi(t')\rangle = 2D_t\delta_{ij}\delta_{xy}\delta(t-t')$. Its strength is identified with $D_t = k_BT/\Gamma$, whereas $\eta_h(t)$ is a white noise term, accounting for the fluctuations in the orientation of the head monomer caused by the environment, with zero mean $\langle \eta_h(t)\rangle = 0$ and variance $\langle \eta_h(t)\eta_h(t')\rangle = 2D_r\delta_1\delta(t-t')$. We have considered different ratios between the translational and rotational diffusion coefficients, $D_t/D_r\sigma^2$, in the simulations.

For not too large noise strengths, the two extreme states, i.e., (i) the linear folding state under shear dominance and (ii) the highly active polymer in the head-out spiraling state, are unresponsive to all fluctuations from the environment [see Figs. 8(a) and 8(b)]. The linear folding state stands out due to the strong shear effects, while the combined action of activity and head chirality ensures the consistency of the head-out spiraling state.

In the complex folding state, Fig. 8(c), where shear- and activity-induced forces are commensurable, the chain state begins to be disrupted by fluctuations. At this point, it is worth noting that if the chain state persists for more than half of the total simulation time despite environmental fluctuations, we deem it to exist under such conditions. Here, the chain state becomes sensitive to the fluctuations above $D_t\tau_0/\sigma^2 \approx 0.2 - D_r\tau_0 \approx 0.5$. The sensitivity stems mostly from the competition between the shear flow and the thermal fluctuations. While the shear flow triggers the folding of the chain and aligns the passive monomers in the shear flow direction, the thermal fluctuations cause their motions to become randomized again. On the other hand, strong rotational noise randomizes the head

orientation of the chain. However, this does not affect the complex folding state much, since this state is predominantly triggered by the shear.

As the activity of the head monomer increases, the chain enters the head-in spiraling state [Fig. 8(d)], becoming more susceptible to fluctuations also below $D_r\tau_0 \approx 0.5$. In particular, at $D_t\tau_0/\sigma^2 = 0.2$ and $D_r\tau_0 \approx 0.6$ in Fig. 8(d), we observe that the fluctuations significantly disrupt the orientation of the head monomer. Indeed, at certain parameters, the active chain still exhibits a spiraling motion, although lacking an explicit head-in conformation. Moreover, upon comparing the two spiraling states [Figs. 8(b) and 8(d)], we discern that not only the high activity but also the shear terms in Eqs. (8)–(10) may contribute to the head-out spiraling against the fluctuations.

In summary, these results suggest that the head chirality of the head monomer can overcome the rotational fluctuations due to its activity if the shear torque also induces sufficient further rotation. However, in the case of relatively weaker activities, the shear effects are precluded by all fluctuations, resulting in the disappearance of one activity-induced state, the head-in spiraling conformation.

IV. CONCLUSIONS

In conclusion, we have studied a flexible polymer chain in shear flow that exhibits some kind of chirality since the head monomer is dragging the rest of the monomers along a prescribed circle. The combination of activity, shear, and chirality leads to a rich morphology of polymer complexes, which includes both folding and spiraling states. The sense of rotation of the whole complex results from a competition between chirality and shear vorticity and can be tuned by activity and shear. Furthermore, we have demonstrated various physical properties of the active polymer chain, such as the radius of the gyration tensor and the shear viscosity, to characterize these morphological states. Particularly, active chiral polymer chains in folding states exhibit shear thinning behavior, attributed to shear-induced stretching and alignment in the shear direction. Spiraling active chiral polymers disrupt the shear thinning character due to the robust activities of the head monomer, resulting in a Newtonian behavior of the chain. Our work builds the first basic step toward a monomer-resolved understanding of the rheological behavior of chiral active polymers.

Our model can be generalized and extended in various directions. First of all, the role of fluctuations should be explored more, in particular non-thermal ones induced by an active bath.[26,27,53,70] Second, the collective effects of many interacting active polymers in shear flow can be studied, leading possibly to distorted worm-blob-like configurations.[2,8] Moreover, it would be interesting to expose active polymers with chirality to confinement[71] or to complex environments such as porous media[72,73] or periodic pillars[74] to see whether chirality can enhance long-time diffusion significantly.

We remark that our simulations currently do not incorporate the hydrodynamic interactions (HIs) for the sake of simplicity, serving as an initial reference to a "dry" system solely influenced by Gaussian white noise. However, theoretical expectations suggest that HI could influence both the conformational and dynamical characteristics of the active polymer chain, contingent upon the nature of the activity. Finally, the insights gained from the presented work can contribute to developing future applications where the active systems are integrated into new technologies.

SUPPLEMENTARY MATERIAL

See the supplementary material for the following: S1.mp4: Linear folding regime ($v_0\tau_0/\sigma = 1$, $\dot{\gamma}\tau_0 = 10$), S2.mp4: Complex folding regime ($v_0\tau_0/\sigma = 10$, $\dot{\gamma}\tau_0 = 2$), S3.mp4: Head-in spiraling regime ($v_0\tau_0/\sigma = 10$, $\dot{\gamma}\tau_0 = 0.05$), S4.mp4: Head-out spiraling regime ($v_0\tau_0/\sigma = 80$, $\dot{\gamma}\tau_0 = 0.1$), S5.mp4: Unstable head-out spiraling regime ($v_0\tau_0/\sigma = 40$, $\dot{\gamma}\tau_0 = 0.1$), and S6.mp4: An example of partially developed polymer structures ($v_0\tau_0/\sigma = 10$, $\dot{\gamma}\tau_0 = 0.1$).

ACKNOWLEDGMENTS

H.L. acknowledges the financial support from the German Research Foundation (DFG) under Project No. LO 418/30-1. The work of A.G.B. was supported within the EU MSCA-ITN ActiveMatter (Proposal No. 812780).

AUTHOR DECLARATIONS

Conflict of Interest

The authors have no conflicts to disclose.

Author Contributions

A. Gülce Bayram: Data curation (equal); Formal analysis (lead); Investigation (lead); Methodology (equal); Software (lead); Validation (lead); Writing – original draft (lead). **Luca Biancofiore**: Conceptualization (equal); Funding acquisition (lead); Project administration (lead); Supervision (lead); Writing – review & editing (equal). **Hartmut Löwen**: Conceptualization (equal); Methodology (equal); Supervision (supporting); Writing – review & editing (equal).

DATA AVAILABILITY

The data that support the findings of this study are available from the corresponding author upon reasonable request.

APPENDIX A: THE EFFECT OF CHAIN LENGTH

We investigate the effect of the polymer chain length on the state diagram. By doubling the number of monomers in the chain ($N_m = 40$), we observe in Fig. 9(a) a notable shift in the conformational states at high activities compared to the existing one ($N_m = 20$). Although we also include the normalization by the number of monomers for the nondimensional activity on the x-axis, a longer polymer chain exhibits a wider region corresponding to the head-in spiraling state. As discussed in Sec. III A, the transition from head-in to head-out spiraling state is determined by the maximum cavity size formed by the chain, which is directly related to the chain length. The discrepancies in the state diagram point out the role of the chain bonds, which allow for further extension of the chain. Consequently, the active chain can continue forming a larger cavity in

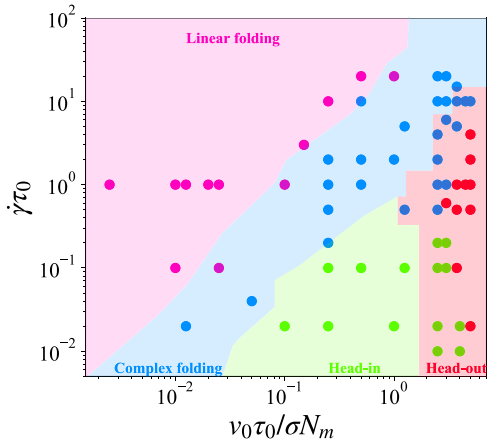

FIG. 9. State diagram normalized by the number of monomers, N_m, for the active polymer chains composed of $N_m = 20$ (represented by the colored background) and $N_m = 40$ (closed symbols). The colorcode represents different states: linear folding (magenta), complex folding (blue), head-in spiraling (green), and head-out spiraling (red).

the head-in spiraling state with increasing activity, thereby shifting the transition to the head-out spiraling states to higher activity levels compared to its shorter polymer counterpart.

We have shown in Fig. 6(b) that a stronger self-propulsion enhances the chain mobility, enabling easier flow for the chain and reducing the viscosity. In addition to that, we also analyze how the length of the chain influences the resistance to flow in Fig. 10. The longer polymer chain ($N_m = 40$) generally exhibits a higher viscosity than $N_m = 20$.

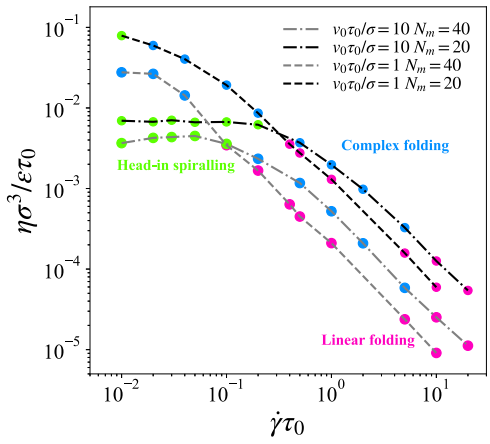

FIG. 10. Comparison of nondimensional shear viscosity $\eta\sigma^3/\varepsilon\tau_0$ of two chain lengths [$N_m = 20$ (black line), $N_m = 40$ (gray line)] as a function of the shear rate $\dot{\gamma}\tau_0$ for the polymer chain activities $v_0\tau_0/\sigma = (10, 1)$. The symbols denote the state of the active polymer chain at the corresponding states: linear folding (magenta), complex folding (blue), head-in spiraling (green), and head-out spiraling (red).

APPENDIX B: EFFECT OF THE HEAD CHIRALITY, ω_c

Here, we present the results illustrating the effect of the chirality of the head monomer on the conformational states of an active polymer chain. The head chirality of the polymer chain is adjusted by modifying the term ω_c in Eq. (2). In the paper, the conformational states have been discussed primarily for the case where $\omega_c\tau_0 = 2$ (see Fig. 2). Now, in Fig. 11, we address two cases, a lower ($\omega_c\tau_0 = 1$) and a higher ($\omega_c\tau_0 = 5$) head chirality.

The folding states are not significantly affected by the head chirality strength. This is simply because the folding states arise from the shear dominance in the system, and the head chirality term ω_c is not directly linked to the shear rate, as shown in Eq. (2). On the other hand, the chiral motion of the polymer chain depends on its activity via the active speed term v_0. This relationship is confirmed by the simulations that the head chirality (different values of ω_c) causes a change in the spiraling states on the state diagram. Comparing Figs. 2 and 11(a), a weaker chirality shifts the head-out spiraling transition to lower activities by limiting the head-in spiraling region. Conversely, a polymer chain with stronger chirality requires a large $v_0\tau_0/\sigma$ to reach the head-out spiraling state, as shown in Fig. 11(b). This indicates that the chirality of the head monomer determines the encapsulation route of the polymer chain at the spiraling state, allowing us to reach the desired state not only by tuning the activity but also the chirality. Although both folding states are not influenced directly as ω_c changes, the shifting of spiraling states to higher activity regions mildly extends the region of complex folding states observed on the state diagram.

This analysis sheds light on the unique effect of the combination of activity and chirality. In particular, the head-in spiraling regime emerges as a distinctive feature of an active polymer chain with a chiral head. This conclusion is further corroborated by the simulation conducted under conditions where the chirality parameter $\omega_c\tau_0$ is set to zero [see Fig. 11(c)]. In this setup, the orientation of the head monomer is solely affected by the vorticity of the shear flow. As a result, the head-in spiraling state completely vanishes, affirming its existence due to the presence of head chirality. Parts of the head-out spiraling are also disrupted for certain parameters, resulting in partially developed structures. Moreover, while the folding states merge on the state diagram, they remain distinguishable based on the level of activity.

However, an alternative non-dimensionalization can be introduced by explicitly incorporating the chirality ω_c. Given that $\tau_0 = 1/\omega_c$, one can define the dimensionless shear rate as $\dot{\gamma}/2\omega_c$, which provides a more direct measure of the competition between chirality and shear. This representation compares the shear-induced rotation rate with the intrinsic rotational dynamics of the chiral particles. A similar rescaling can be applied to the activity, yielding a dimensionless form, $v_0/\sigma\omega_c$, which normalizes the active effects by the chirality.

This rescaling provides useful physical intuition by facilitating a direct comparison of different chiralities. In particular, it allows us to better compare the state diagrams for different chiralities, revealing that, under this non-dimensionalization, all state diagrams collapse into the same universal form (see Fig. 12).

We further investigate the impact of chirality on the viscosity of a polymer chain under varying activity levels and shear rates, see Fig. 13. Our findings indicate that chirality significantly influences

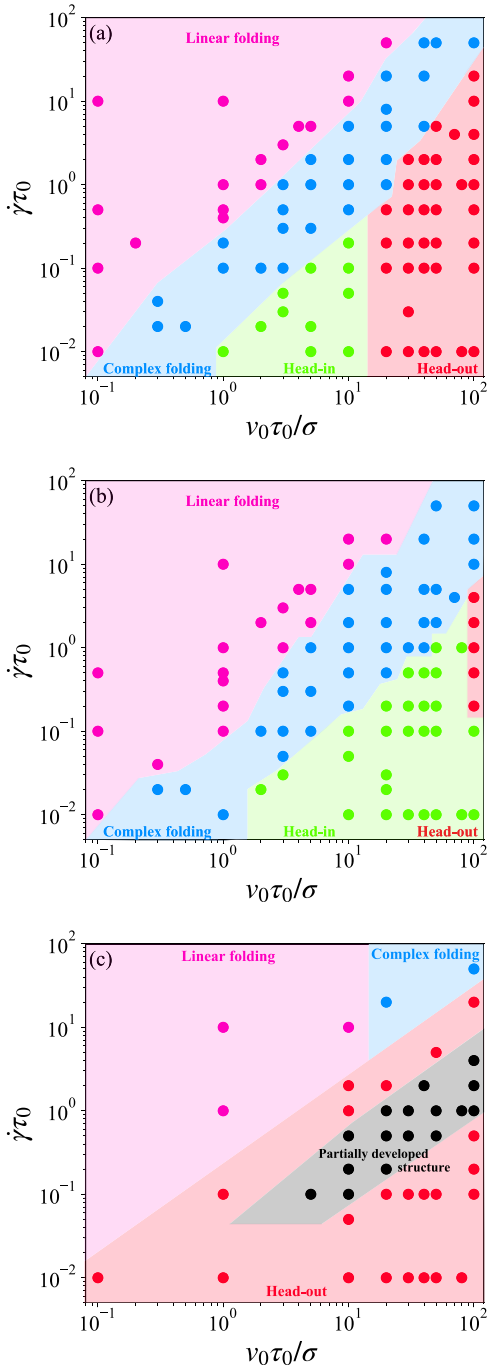

FIG. 11. State diagrams of the active polymer chain as a function of activity $v_0\tau_0/\sigma$ and shear rates $\dot{\gamma}\tau_0$ when the chirality of the head monomer is set to (a) $\omega_c\tau_0 = 1$, (b) $\omega_c\tau_0 = 5$, and (c) $\omega_c\tau_0 = 0$. The colorcode represents different states: linear folding (magenta), complex folding (blue), head-in spiraling (green), head-out spiraling (red), and partially developed structure (black).

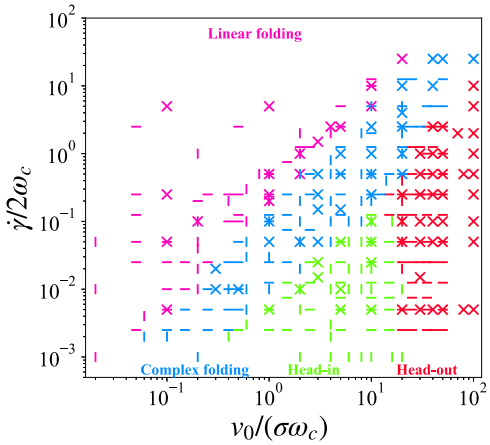

FIG. 12. State diagram of the active polymer chain conformations as a function of activity $v_0/\sigma\omega_c$ and shear rate $\dot{\gamma}/2\omega_c$ for $\omega_c\tau_0 = 1$ (X), $\omega_c\tau_0 = 2$ (–), and $\omega_c\tau_0 = 5$ (|): linear folding (magenta), complex folding (blue), head-in spiraling (green), and head-out spiraling (red).

viscosity, particularly for spiraling chains. As activity increases, the enhanced self-propulsion of monomers leads to more frequent reorientations and deformations, amplifying the overall impact of chirality on viscosity. In addition, the spiraling motion contributes to a reduction in resistance to flow. This effect is particularly evident for the chain with $\dot{\gamma}\tau_0 = 0.01$ and $v_0\tau_0/\sigma = 10$. However, this effect diminishes for chains in folded states where the shear rate increases or activity decreases. All these results are in line with our observations in Fig. 7 of this paper.

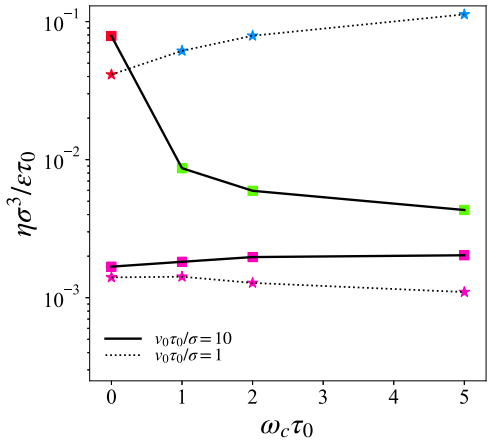

FIG. 13. Nondimensional shear viscosity $\eta\sigma^3/\varepsilon\tau_0$ as a function of head chirality $\omega_c\tau_0$ for activities $v_0\tau_0/\sigma = (1, 10)$ subjected to shear rates $\dot{\gamma}\tau_0 = 1$ (star) and $\dot{\gamma}\tau_0 = 0.01$ (square). The colorcode for the symbols represents different states: linear folding (magenta), complex folding (blue), head-in spiraling (green), and head-out spiraling (red).

REFERENCES

[1] R. G. Winkler, J. Elgeti, and G. Gompper, "Active polymers—Emergent conformational and dynamical properties: A brief review," J. Phys. Soc. Jpn. **86**, 101014 (2017).
[2] A. Deblais, K. R. Prathyusha, R. Sinaasappel, H. Tuazon, I. Tiwari, V. P. Patil, and M. S. Bhamla, "Worm blobs as entangled living polymers: From topological active matter to flexible soft robot collectives," Soft Matter **19**, 7057–7069 (2023).
[3] A. Ghosh and N. S. Gov, "Dynamics of active semiflexible polymers," Biophys. J. **107**, 1065–1073 (2014).
[4] S. Ramaswamy, "The mechanics and statistics of active matter," Annu. Rev. Condens. Matter Phys. **1**, 323–345 (2010).
[5] P. Romanczuk, M. Bär, W. Ebeling, B. Lindner, and L. Schimansky-Geier, "Active brownian particles: From individual to collective stochastic dynamics," Eur. Phys. J.: Spec. Top. **202**, 1–162 (2012).
[6] C. Bechinger, R. Di Leonardo, H. Löwen, C. Reichhardt, G. Volpe, and G. Volpe, "Active particles in complex and crowded environments," Rev. Mod. Phys. **88**, 045006 (2016).
[7] A. Zöttl and H. Stark, "Emergent behavior in active colloids," J. Phys.: Condens. Matter **28**, 253001 (2016).
[8] V. P. Patil, H. Tuazon, E. Kaufman, T. Chakrabortty, D. Qin, J. Dunkel, and M. S. Bhamla, "Ultrafast reversible self-assembly of living tangled matter," Science **380**, 392–398 (2023).
[9] A. Deblais, S. Woutersen, and D. Bonn, "Rheology of entangled active polymer-like T. Tubifex worms," Phys. Rev. Lett. **124**, 188002 (2020).
[10] A. Biswas and A. Kudrolli, "Escape dynamics of confined undulating worms," Soft Matter **19**, 4376–4384 (2023).
[11] A. R. Bausch and K. Kroy, "A bottom-up approach to cell mechanics," Nat. Phys. **2**, 231–238 (2006).
[12] F. Bonacci, B. Chakrabarti, D. Saintillan, O. Du Roure, and A. Lindner, "Dynamics of flexible filaments in oscillatory shear flows," J. Fluid Mech. **955**, A35 (2023).
[13] S. K. Anand and S. P. Singh, "Structure and dynamics of a self-propelled semiflexible filament," Phys. Rev. E **98**, 042501 (2018).
[14] C. Scholz, A. Ldov, T. Pöschel, M. Engel, and H. Löwen, "Surfactants and rotelles in active chiral fluids," Sci. Adv. **7**, eabf8998 (2021).
[15] R. Chelakkot, A. Gopinath, L. Mahadevan, and M. F. Hagan, "Flagellar dynamics of a connected chain of active, polar, brownian particles," J. R. Soc. Interface **11**, 20130884 (2014).
[16] J. Yan, M. Han, J. Zhang, C. Xu, E. Luijten, and S. Granick, "Reconfiguring active particles by electrostatic imbalance," Nat. Mater. **15**, 1095–1099 (2016).
[17] M. Shafiei Aporvari, M. Utkur, E. U. Saritas, G. Volpe, and J. Stenhammar, "Anisotropic dynamics of a self-assembled colloidal chain in an active bath," Soft Matter **16**, 5609–5614 (2020).
[18] A. Kaiser, S. Babel, B. ten Hagen, C. von Ferber, and H. Löwen, "How does a flexible chain of active particles swell?," J. Chem. Phys. **142**, 124905 (2015).
[19] E. Lawson-Keister, "Heterotypic interactions in the complex environments of living tissue," Ph.D. thesis, Syracuse University, 2023.
[20] Y. Shelke, F. Camerin, S. Marín-Aguilar, R. W. Verweij, M. Dijkstra, and D. J. Kraft, "Flexible colloidal molecules with directional bonds and controlled flexibility," ACS Nano **17**, 12234–12246 (2023).
[21] J. Melio, S. Riedel, A. Azadbakht, S. A. Caipa Cure, T. M. J. Evers, M. Babaei, A. Mashaghi, J. de Graaf, and D. J. Kraft, Soft Matter **21**, 2541–2547 (2025).
[22] K. Becker, C. Teeple, N. Charles, Y. Jung, D. Baum, J. C. Weaver, L. Mahadevan, and R. Wood, "Active entanglement enables stochastic, topological grasping," Proc. Natl. Acad. Sci. U. S. A. **119**, e2209819119 (2022).
[23] G. Volpe, I. Buttinoni, D. Vogt, H.-J. Kümmerer, and C. Bechinger, "Microswimmers in patterned environments," Soft Matter **7**, 8810–8815 (2011).
[24] B. Ten Hagen, F. Kümmel, R. Wittkowski, D. Takagi, H. Löwen, and C. Bechinger, "Gravitaxis of asymmetric self-propelled colloidal particles," Nat. Commun. **5**, 4829 (2014).
[25] S.-N. Lin, W.-C. Lo, and C.-J. Lo, "Dynamics of self-organized rotating spiral-coils in bacterial swarms," Soft Matter **10**, 760–766 (2014).
[26] J. Harder, C. Valeriani, and A. Cacciuto, "Activity-induced collapse and reexpansion of rigid polymers," Phys. Rev. E **90**, 062312 (2014).
[27] A. Kaiser and H. Löwen, "Unusual swelling of a polymer in a bacterial bath," J. Chem. Phys. **141**, 044903 (2014).
[28] R. E. Isele-Holder, J. Elgeti, and G. Gompper, "Self-propelled worm-like filaments: Spontaneous spiral formation, structure, and dynamics," Soft Matter **11**, 7181–7190 (2015).
[29] S. Mandal, C. Kurzthaler, T. Franosch, and H. Löwen, "Crowding-enhanced diffusion: An exact theory for highly entangled self-propelled stiff filaments," Phys. Rev. Lett. **125**, 138002 (2020).
[30] T. Eisenstecken, G. Gompper, and R. Winkler, "Conformational properties of active semiflexible polymers," Polymers **8**, 304 (2016).
[31] I. Saha Dalal, A. Albaugh, N. Hoda, and R. G. Larson, "Tumbling and deformation of isolated polymer chains in shearing flow," Macromolecules **45**, 9493–9499 (2012).
[32] R. G. Winkler, "Semiflexible polymers in shear flow," Phys. Rev. Lett. **97**, 128301 (2006).
[33] D. Das and S. Sabhapandit, "Accurate statistics of a flexible polymer chain in shear flow," Phys. Rev. Lett. **101**, 188301 (2008).
[34] G.-L. He, R. Messina, H. Löwen, A. Kiriy, V. Bocharova, and M. Stamm, "Shear-induced stretching of adsorbed polymer chains," Soft Matter **5**, 3014–3017 (2009).
[35] G.-L. He, R. Messina, and H. Löwen, "Waddling and somersault motion of an adsorbed polymer in external fields," Europhys. Lett. **93**, 18002 (2011).
[36] C. Aust, M. Kröger, and S. Hess, "Structure and dynamics of dilute polymer solutions under shear flow via nonequilibrium molecular dynamics," Macromolecules **32**, 5660–5672 (1999).
[37] R. G. Winkler, "Dynamics of flexible active brownian dumbbells in the absence and the presence of shear flow," Soft Matter **12**, 3737–3749 (2016).
[38] A. Martín-Gómez, G. Gompper, and R. G. Winkler, "Active brownian filamentous polymers under shear flow," Polymers **10**, 837 (2018).
[39] N. Küchler, H. Löwen, and A. M. Menzel, "Getting drowned in a swirl: Deformable bead-spring model microswimmers in external flow fields," Phys. Rev. E **93**, 022610 (2016).
[40] R. G. Winkler and G. Gompper, "The physics of active polymers and filaments," J. Chem. Phys. **153**, 040901 (2020).
[41] A. J. T. M. Mathijssen, T. N. Shendruk, J. M. Yeomans, and A. Doostmohammadi, "Upstream swimming in microbiological flows," Phys. Rev. Lett. **116**, 028104 (2016).
[42] R. W. Nash, R. Adhikari, J. Tailleur, and M. E. Cates, "Run-and-tumble particles with hydrodynamics: Sedimentation, trapping, and upstream swimming," Phys. Rev. Lett. **104**, 258101 (2010).
[43] A. J. T. M. Mathijssen, N. Figueroa-Morales, G. Junot, É. Clément, A. Lindner, and A. Zöttl, "Oscillatory surface rheotaxis of swimming *E. coli* bacteria," Nat. Commun. **10**, 3434 (2019).
[44] H. M. López, J. Gachelin, C. Douarche, H. Auradou, and E. Clément, "Turning bacteria suspensions into superfluids," Phys. Rev. Lett. **115**, 028301 (2015).
[45] A. G. Bayram, F. J. Schwarzendahl, H. Löwen, and L. Biancofiore, "Motility-induced shear thickening in dense colloidal suspensions," Soft Matter **19**, 4571–4578 (2023).
[46] H. Ahmed and L. Biancofiore, "A new approach for modeling viscoelastic thin film lubrication," J. Non-Newtonian Fluid Mech. **292**, 104524 (2021).
[47] H. Ahmed and L. Biancofiore, "A modified viscosity approach for shear thinning lubricants," Phys. Fluids **34**, 103103 (2022).
[48] B. Liebchen and D. Levis, "Chiral active matter," Europhys. Lett. **139**, 67001 (2022).
[49] L. Caprini, I. Abdoli, U. M. B. Marconi, and H. Löwen, "Spontaneous self-wrapping in chiral active polymers," arXiv:2410.02567 (2024).
[50] S. K. Anand, "A computer simulation study of a chiral active ring polymer," J. Chem. Phys. **161**, 184901 (2024).
[51] H. Löwen, "Chirality in microswimmer motion: From circle swimmers to active turbulence," Eur. Phys. J.: Spec. Top. **225**, 2319–2331 (2016).
[52] F. Kümmel, B. Ten Hagen, R. Wittkowski, I. Buttinoni, R. Eichhorn, G. Volpe, H. Löwen, and C. Bechinger, "Circular motion of asymmetric self-propelling particles," Phys. Rev. Lett. **110**, 198302 (2013).
[53] D. Grober, I. Palaia, M. C. Uçar, E. Hannezo, A. Šarić, and J. Palacci, "Unconventional colloidal aggregation in chiral bacterial baths," Nat. Phys. **19**, 1680–1688 (2023).

[54]K. Kruse, J.-F. Joanny, F. Jülicher, J. Prost, and K. Sekimoto, "Asters, vortices, and rotating spirals in active gels of polar filaments," Phys. Rev. Lett. **92**, 078101 (2004).
[55]H. H. Wensink, J. Dunkel, S. Heidenreich, K. Drescher, R. E. Goldstein, H. Löwen, and J. M. Yeomans, "Meso-scale turbulence in living fluids," Proc. Natl. Acad. Sci. **109**, 14308–14313 (2012).
[56]H. H. Wensink and H. Löwen, "Emergent states in dense systems of active rods: From swarming to turbulence," J. Phys.: Condens. Matter **24**, 464130 (2012).
[57]Z. Dunajova, B. P. Mateu, P. Radler, K. Lim, D. Brandis, P. Velicky, J. G. Danzl, R. W. Wong, J. Elgeti, E. Hannezo, and M. Loose, "Chiral and nematic phases of flexible active filaments," Nat. Phys. **19**, 1916–1926 (2023).
[58]S. Van Teeffelen and H. Löwen, "Dynamics of a Brownian circle swimmer," Phys. Rev. E **78**, 020101 (2008).
[59]A. Kaiser and H. Löwen, "Vortex arrays as emergent collective phenomena for circle swimmers," Phys. Rev. E **87**, 032712 (2013).
[60]B. Ten Hagen, R. Wittkowski, and H. Löwen, "Brownian dynamics of a self-propelled particle in shear flow," Phys. Rev. E **84**, 031105 (2011).
[61]J. K. Dhont, *An Introduction to Dynamics of Colloids* (Elsevier, 1996).
[62]A. R. Sprenger, M. A. Fernandez-Rodriguez, L. Alvarez, L. Isa, R. Wittkowski, and H. Löwen, "Active Brownian motion with orientation-dependent motility: Theory and experiments," Langmuir **36**, 7066–7073 (2020).
[63]R. Huhnstock, M. Reginka, A. Tomita, M. Merkel, K. Dingel, D. Holzinger, B. Sick, M. Vogel, and A. Ehresmann, "Translatory and rotatory motion of exchange-bias capped Janus particles controlled by dynamic magnetic field landscapes," Sci. Rep. **11**, 21794 (2021).
[64]M. Y. Ben Zion, Y. Caba, A. Modin, and P. M. Chaikin, "Cooperation in a fluid swarm of fuel-free micro-swimmers," Nat. Commun. **13**, 184 (2022).
[65]M. Rey, G. Volpe, and G. Volpe, "Light, matter, action: Shining light on active matter," ACS Photonics **10**, 1188–1201 (2023).
[66]J. D. Weeks, D. Chandler, and H. C. Andersen, "Role of repulsive forces in determining the equilibrium structure of simple liquids," J. Chem. Phys. **54**, 5237–5247 (1971).
[67]K. Kremer and G. S. Grest, "Dynamics of entangled linear polymer melts: A molecular-dynamics simulation," J. Chem. Phys. **92**, 5057–5086 (1990).
[68]A. Panda, R. G. Winkler, and S. P. Singh, "Characteristic features of self-avoiding active Brownian polymers under linear shear flow," Soft Matter **19**, 8577–8586 (2023).
[69]M. Rubinstein and R. H. Colby, *Polymer Physics* (Oxford University Press, 2003).
[70]J. Shin, A. G. Cherstvy, W. K. Kim, and R. Metzler, "Facilitation of polymer looping and giant polymer diffusivity in crowded solutions of active particles," New J. Phys. **17**, 113008 (2015).
[71]A. B. Yıldırım, A. Erbaş, and L. Biancofiore, "Molecular rheology of nanoconfined oligomer melts," J. Rheol. **68**, 285–299 (2024).
[72]L. Theeyancheri, S. Chaki, T. Bhattacharjee, and R. Chakrabarti, "Active dynamics of linear chains and rings in porous media," J. Chem. Phys. **159**, 014902 (2023).
[73]C. Kurzthaler, S. Mandal, T. Bhattacharjee, H. Löwen, S. S. Datta, and H. A. Stone, "A geometric criterion for the optimal spreading of active polymers in porous media," Nat. Commun. **12**, 7088 (2021).
[74]M. Fazelzadeh, Q. Di, E. Irani, Z. Mokhtari, and S. Jabbari-Farouji, "Active motion of tangentially driven polymers in periodic array of obstacles," J. Chem. Phys. **159**, 224903 (2023).